



Elastic Modulus Evolution and Behavior of Si/Mullite/BSAS-Based Environmental Barrier Coatings Exposed to High Temperature in Water Vapor Environment

C.V. Cojocaru, S.E. Kruger, C. Moreau, and R.S. Lima

(Submitted May 14, 2010; in revised form October 22, 2010)

Si-based ceramics (e.g., SiC and Si₃N₄) are known as promising high-temperature structural materials in various components where metals/alloys reached their ultimate performances (e.g., advanced gas turbine engines and structural components of future hypersonic vehicles). To alleviate the surface recession that Si-based ceramics undergo in a high-temperature environmental attack (e.g., H₂O vapor), appropriate refractory oxides are engineered to serve as environmental barrier coatings (EBCs). The current state-of-the-art EBCs multilayer system comprises a silicon (Si) bond coat, mullite (3Al₂O₃·2SiO₂) interlayer and (1 - x)BaO·xSrO·Al₂O₃·2SiO₂, 0 ≤ x ≤ 1 (BSAS) top coat. In this article, the role of high-temperature exposure (1300 °C) performed in H₂O vapor environment (for time intervals up to 500 h) on the elastic moduli of air plasma sprayed Si/mullite/BSAS layers deposited on SiC substrates was investigated via depth-sensing indentation. Laser-ultrasonics was employed to evaluate the *E* values of as-sprayed BSAS coatings as an attempt to validate the indentation results. Fully crystalline, crack-free, and near-crack-free as-sprayed EBCs were engineered under controlled deposition conditions. The absence of phase transformation and stability of the low elastic modulus values (e.g., ~60-70 GPa) retained by the BSAS top layers after harsh environmental exposure provides a plausible explanation for the almost crack-free coatings observed. The relationships between the measured elastic moduli of the EBCs and their microstructural behavior during the high-temperature exposure are discussed.

Keywords BSAS, elastic modulus, environmental barrier coatings, heat-exposure, mullite, water vapor

1. Introduction

To increase the efficiency of a gas turbine engine, higher operating temperatures are needed. At the same time, the durability of the engine components must correspondingly sustain the temperature increase. While metal super alloys are widely used for various engine components, alternative materials and in particular silicon (Si)-based ceramics (e.g., SiC and Si₃N₄) emerged for

This article is an invited paper selected from presentations at the 2010 International Thermal Spray Conference and has been expanded from the original presentation. It is simultaneously published in *Thermal Spray: Global Solutions for Future Applications, Proceedings of the 2010 International Thermal Spray Conference*, Singapore, May 3-5, 2010, Basil R. Marple, Arvind Agarwal, Margaret M. Hyland, Yuk-Chiu Lau, Chang-Jiu Li, Rogerio S. Lima, and Ghislain Montavon, Ed., ASM International, Materials Park, OH, 2011.

C.V. Cojocaru, S.E. Kruger, C. Moreau, and R.S. Lima, National Research Council of Canada (NRC), Industrial Materials Institute (IMI), Boucherville, QC, Canada. Contact e-mail: cristian.cojocaru@cnrc-nrc.gc.ca.

high-temperature applications due to their high mechanical strengths at high temperatures and density values in the order of 1/3 of those of metallic superalloys. For most of these applications, protective coatings are often beneficial and even required. Layered refractory oxide coatings offering a suitable thermal-insulation reduce the thermal gradient through the structural component and increase its durability. Coatings for components formed of Si-based materials must fulfill an important coincident role namely to provide an environmental protection against water vapors and corrosive molten aluminosilicates. Thus these coatings have been named environmental barrier coatings (EBCs) (Ref 1-6).

In gas turbines, a low permeability for water vapors is a critical characteristic for an EBC system so as to inhibit the formation of silicon hydroxide (Si(OH)₄) gas by the reaction of the water vapor originating from the jet fuel combustion with the SiO₂ scale formed on the Si-based substrate (Ref 1-6). Future hypersonic vehicles flying in low Earth orbit will also employ Si-based materials on their external structure. In this case, due to the low O₂ pressure at high altitudes and high temperatures caused by the friction with the atmosphere during ascending and re-entry, gaseous silicon monoxide (SiO) will tend to form and volatilize. Under these conditions the surface of Si-based substrates would recess and therefore, EBCs will be needed to protect the external structure of hypersonic vehicles (Ref 7).

In brief, the requirements for an efficient EBC system in these applications could be outlined as follows: (i) good chemical compatibility and good adherence [offered mainly by a coefficient of thermal expansion (CTE) match] with the substrate, (ii) low thermal conductivity, (iii) crack resistance (offered by phase stability, low stress, i.e., low elastic modulus and sintering resistance), and specifically for gas turbines, (iv) H₂O vapor stability and durability for molten aluminosilicate corrosion (Ref 1-7).

The current state-of-the-art EBC system, which satisfies the four requirements mentioned above, comprises a Si bond coat, a mullite (3Al₂O₃·2SiO₂) interlayer, and a (1 - x)BaO·xSrO·Al₂O₃·2SiO₂, 0 ≤ x ≤ 1 (BSAS) crack-resistant, and water vapor attack resistant top coat (Ref 1-4). Evaluating and understanding EBCs mechanical properties, such as the elastic modulus and the strain-stress relationship, are essential for their practical application and reliable employment.

Concerning the BSAS top coat, the monoclinic celsian phase was found to be the most desirable due to its stability and low CTE (i.e., 4.0-5.15 × 10⁻⁶/°C and thus a close match with SiC, 4.02 × 10⁻⁶/°C). Consequently, studies on phase evolution of BSAS in environmental barrier coatings represented a major point of interest and were reported in Ref 8-11. More recently, using x-ray synchrotron radiation experiments and modelling, Harder et al. (Ref 12) investigated residual stresses in doped aluminosilicate multilayer coatings on melt infiltrated SiC ceramic matrix composites. It was demonstrated that tensile strains due to CTE mismatch between a hexacelsian (CTE 7.5-8 × 10⁻⁶/°C) topcoat and the underlying layers caused through-thickness cracking. Nevertheless, the elastic properties of as-sprayed and thermally treated Si/mullite/BSAS EBCs in water vapor environment and the evolution of phase composition of thermally sprayed BSAS have been scarcely reported in the literature. Furthermore, to the best knowledge of the authors, this is the first report on atmospheric plasma spray (APS) direct formation of celsian-type BSAS coatings achieved without any initial crystallization of a metastable hexacelsian (and basically detrimental) phase.

In this study, the role of high-temperature treatment (1300 °C) in H₂O vapor environment on the evolution of the phase content and elastic modulus of air plasma sprayed crystalline Si/mullite/BSAS EBCs deposited on SiC substrates was investigated via depth sensing indentation. Laser-ultrasonics was employed to evaluate the *E* values of as-sprayed BSAS coating to validate the indentation results.

2. Experimental

2.1 Sample Preparation

The powders employed in this study were the following: (i) silicon (Si)—fused and crushed (Si-1168, Cerac Inc., Milwaukee, WI, USA), (ii) mullite—fused and crushed (3Al₂O₃·2SiO₂) (M_SG) (#1020, Saint-Gobain Worchester, MA, USA), and (iii) barium strontium alumina

silicate—spray-dried (BaO-SrO-Al₂O₃-SiO₂) (BSAS) (Amperit 870.084, H.C Starck, Newton, MA, USA). Prior to spraying, the phase composition of each powder was determined via x-ray diffraction (XRD) (D8-Discovery, Bruker AXS Inc., Madison, WI, USA) using Cu Kα radiation in Bragg-Brentano (θ-2θ) configuration. The powder morphology was analyzed via scanning electron microscopy (SEM). The particle size distribution for each powder was evaluated using a laser scattering particle size analyzer (LS 13320, Beckman Coulter, Miami, FL, USA). Their respective *d*₁₀, *d*₅₀, and *d*₉₀ (i.e., % vol. of the particles showing diameters smaller than their values) are given in the Table 1.

Using an air plasma spray (APS) torch (Axial III, Northwest Mettech, North Vancouver, BC, Canada), the powders were sprayed onto 5 cm × 5 cm sintered α-SiC substrates (Hexaloy SA, Saint-Gobain, Niagara Falls, MA, USA). The Axial III Plasma Spray Torch is a three anode-three cathode plasma torch with axial injection feed of the powder. In-flight particle temperature and velocity values were measured using a dedicated optical sensor (DPV 2000, Tecnar Automation, St-Bruno, QC, Canada) and the substrate temperature monitored with an infrared camera (SC 620, FLIR Systems AB, Danderyd, Sweden). Coatings were deposited using proprietary spray conditions making it possible to produce fully crystalline as-sprayed coatings.

2.2 Structural Characterization

As a general sample preparation procedure, the 5 cm × 5 cm coupons were cut in quarters for thermal exposure and structural/mechanical analysis. EBC performance was evaluated using an in-house developed test rig based on a high-temperature tube furnace (STT-1700-2.0-18, SentroTech, Berea, OH, USA). Thermal exposure tests were performed at 1300 °C (1 atm) in a continuous flow (~3.5 cm/s) of H₂O vapor (90% H₂O/10% air) in an attempt to simulate the lean environment of a gas turbine (Ref 1, 2) for time intervals up to 500 h.

The crystallinity of the as-sprayed and thermally exposed coatings was analyzed via (θ-2θ) x-ray diffraction with a scanning step size of 0.02° and a 2.5 s/step acquisition time through a 1° fine collimator slit.

Samples were embedded in epoxy prior to cross section cutting and further prepared by standard metallography procedures for SEM (S4700, Hitachi, Tokyo, Japan) analysis and instrumented indentation testing (IIT) (Nanoindenter G200, Agilent Technologies, Oak Ridge, TN, USA).

Porosity of each coating forming the tri-layer structures (both as-sprayed and thermally exposed) was measured

Table 1 Particle size distribution of Si, mullite, and BSAS powders determined via laser-scattering analysis

Powder, μm	Si	M_SG	BSAS
<i>d</i> ₁₀	1	15	20
<i>d</i> ₅₀	16	30	53
<i>d</i> ₉₀	40	50	86

using image analysis (IA) of SEM micrographs recorded in backscattered mode. One sample was analyzed per coating and more than 20 cross section SEM images per coating were captured (at magnifications of 500× and 1k×) and further “binarized.” Porosity was measured as area percentage of dark features (pores) using Visilog 3.5 image analysis software.

2.3 *E* Measurements Via Instrumented Indentation Testing

Using depth-sensing indentation (Oliver-Pharr method) (Ref 13) with a Berkovich diamond tip, the elastic modulus (*E*) values of each deposited coating were measured at room temperature on the polished cross section of the samples. Since the applied indentation loads and their corresponding penetration depths are measured continuously during a loading-unloading cycle, the residual hardness impression does not have to be directly imaged as in conventional microhardness testing. This represents one of the main advantages over the more traditional indentation measurements.

Measurements were performed at loads between 10 and 500 mN with loading times of 15 s and unloading (90% of the segment recorded) times of 20 s. For each coating several sets of 15-20 indents were performed generally spaced at distances correlated with the load applied. The *E* values of the material are calculated based on the initial portion of the unloading curve as the unloading is the purely elastic recovery process. This gives the elastic stiffness of the contact *S* and serves to initially determine the reduced elastic modulus (*E_r*) (with a numerical factor $\beta = 1$ for the triangular cross sections like the Berkovich tip):

$$S = \frac{dP}{dh}$$

where *P* is the load applied on the test surface and *h* is the indenter displacement and

$$E_r = \frac{S\sqrt{\pi}}{2\beta\sqrt{A}}$$

where *A* is the projected area at that load. The *E* value of the test specimen is calculated making use of the reduced *E_r* using the formula:

$$\frac{1}{E_r} = \frac{(1 - \nu^2)}{E} + \frac{(1 - \nu_i^2)}{E_i}$$

where *E_i* = 1141 GPa and Poisson's ratio $\nu_i = 0.07$ are the indenter diamond tip properties used for calculations. In these measurements, the Poisson ratio of the tested coatings was assumed to be 0.25, which is a typical value for ceramic materials. In fact, such estimation ($\nu = 0.25 \pm 0.1$) produces only about a 5% uncertainty in the calculated value of *E* for most materials. More detailed information about this methodology can be found elsewhere (Ref 13).

Four different loads (i.e., 10, 100, 250, and 500 mN) were applied either in form of arrays or on selected locations. Areas with high porosity were intentionally

avoided. Indentations were made on all coatings and also on the substrate. Residual indentation impressions made in the as-sprayed mullite and BSAS coatings with a 500 mN load are depicted in the SEM micrographs shown in Fig. 1.

Surface polishing of the cross sectioned ceramics is a delicate issue. The so-called pull-outs or voids are produced in the surface and indentations are not always easy to position due to an increased porosity. However, suitably dense areas were chosen to be indented but, nevertheless, the porosity that might lie underneath the indent location cannot be predicted or avoided.

2.4 Laser-Ultrasonics Measurement of *E* Values

Elastic modulus value of a BSAS single layer sprayed directly on a SiC substrate was also determined via a laser-based ultrasonic technique to compare the former with the values obtained via instrumented indentation testing (IIT). Elastic modulus was calculated from the ultrasonic velocity measured using a laser-ultrasonic experimental set-up equipped with a pulsed Nd:YAG laser (3rd harmonic: 355 nm wavelength, 35 ps pulse duration) employed to generate surface acoustic waves. This generation laser, in the ultraviolet wavelength with very short pulse duration, is chosen to get optimal generation efficiency. For the detection, a long-pulsed Nd:YAG laser (1064 nm wavelength, 200 μs pulse duration) was coupled to a GaAs photorefractive interferometer by optical fibers. This photorefractive interferometer provides enhanced sensitivity on unpolished surfaces and reliable response to lower ultrasonic frequencies. A detailed set-up description of laser ultrasonic measurements of elastic constants on coatings is given in Ref 14.

3. Results and Discussion

3.1 Microstructural Analysis

XRD patterns reveal the fully crystalline nature of the as-sprayed Si bond coat, mullite, and BSAS coatings (Fig. 2). No amorphous or foreign phases were detected (e.g., γ -alumina in mullite) within the detectability limit of the D8 Discovery XRD set-up (i.e., ~2%) and for the time interval of the performed measurement (i.e., total time of scanning of 1 h/sample). Energy-dispersive x-ray (EDX) chemical analysis (not shown) did not reveal foreign elements in either mullite or BSAS coatings (within 1% detectability limit).

Only the celsian phase observed in the BSAS powder has been found in the as-sprayed BSAS coating as depicted in Fig. 2. Moreover, after the thermal exposures in water vapor at 1300 °C up to 500 h, the celsian phase was preserved and detected. This result demonstrates the high stability of the phase of fully crystalline BSAS coatings (celsian phase) in water vapor environments making it a material of choice as a state-of-the-art EBC coating.

The SEM micrograph of the as-sprayed EBC (Fig. 3a) shows that the Si bond coat appears as a dense and

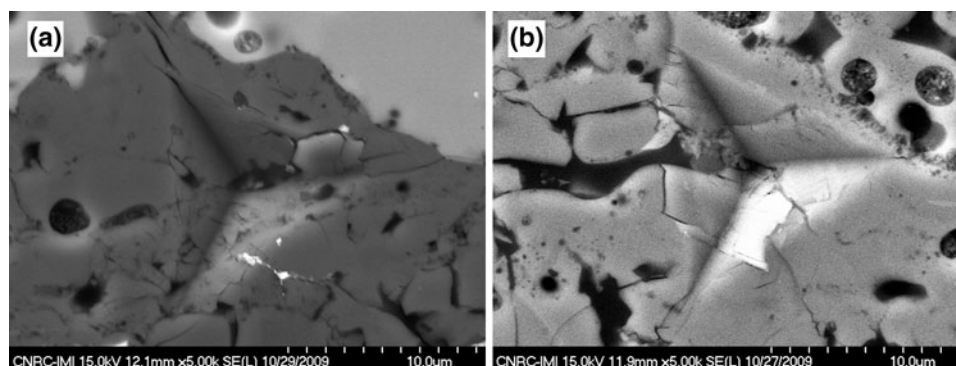


Fig. 1 Indentation testing residual impressions made with a Berkovich diamond tip into (a) mullite and (b) BSAS layers for 500 mN (50 gf) load

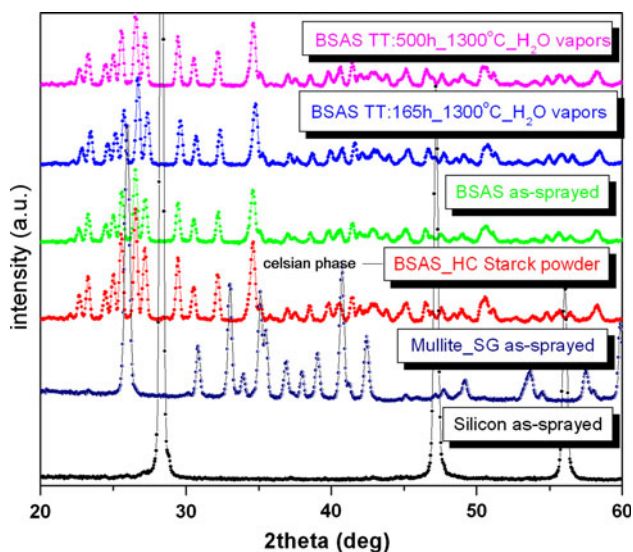


Fig. 2 XRD patterns of atmospheric plasma sprayed Si/mullite/BSAS EBCs

crack-free layer exhibiting good adhesion (i.e., no gaps) to the substrate and to the upper crack-free mullite intermediate layer. Moreover, a very good adhesion between the mullite layer and the near-crack-free BSAS top coat is observed. In the EBC specimens exposed to 1300 °C for extended hours, the formation of pores in the mullite coating next to the Si bond coat interface was detected as shown in Fig. 3(b) and (c). Such a porosity increase has been previously reported and was attributed to the corrosion due to the water vapor (Ref 1), which probably penetrated through the coating porosity.

The SEM cross sections in Fig. 3 show also a high degree of melting for the powders used to deposit the coatings. The entire size distribution of the powders was fully melted and a very strong cohesion between the splats is observed. The porosities for mullite coatings, both as-sprayed and thermally exposed to 1300 °C, were found in the range of 11% ($\pm 1\%$ standard error of the mean). A swift visual inspection of the micrographs from Fig. 3 reveals that the pore size in the mullite coating is much

smaller than in the BSAS coatings. For the BSAS top coat porosity was found in the range of 12% ($\pm 1\%$ standard error of the mean) showing a rather steady behavior with the annealing time period. It appears that the thermal treatment at 1300 °C up to 500 h has small effect on the degree of sintering of these coatings. Nonetheless, it is important to point out that for all EBC specimens exposed to 1300 °C, no debonding, delamination, or major cracking was observed after 500 h of isothermal treatment. Thermal cycling testing, in a H₂O vapor environment, is currently underway so as to assess the mechanical behavior and performance of similar multilayer EBCs. The results will be reported in a future publication.

3.2 Interfaces

When the interface of the as-sprayed Si bond coat and SiC substrate of the tri-layer EBC is observed at higher magnifications, it is possible to notice the presence of a thin silica layer ($\sim 0.5 \mu\text{m}$), Fig. 4(a). No significant growth of this silica layer was observed after an exposure at 1300 °C for 165 h (Fig. 4b) and 500 h (Fig. 4c) in water vapor environment. However, the uncoated surface of the substrate (Fig. 5) exhibits a much thicker ($\sim 5 \mu\text{m}$) and low-adherent SiO₂ layer (composition verified by EDX). Therefore, the EBC system produced in this study protected effectively the SiC substrate against oxidation and water vapor attack, showing the same trend also observed by other authors (Ref 1-5).

3.3 Mechanical Testing Via IIT and the Indentation Size Effect

The influence of indentation load on E and hardness values of ceramics has been investigated by several groups and it was reported that both exhibit significant dependence on the indentation load (Ref 15). A general trend is that elastic moduli tend to decrease with the increase of the load applied (Ref 16). To investigate these phenomena, measurements were performed on the deposited coatings by varying the indentation loads from 10 to 500 mN to search for the interval values of the applied force at which the E data obtained tends to stabilize. As shown in Fig. 6, E values started to exhibit this trend

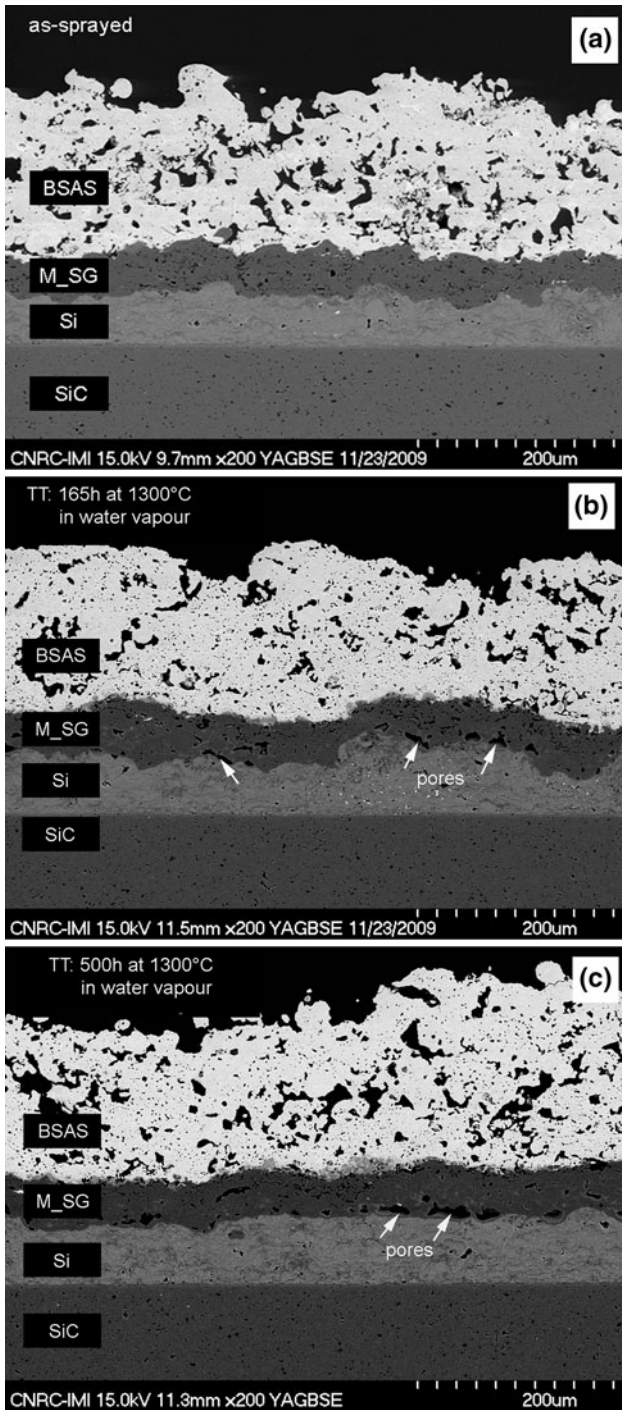


Fig. 3 SEM micrographs of the Si/mullite/BSAS EBCs before and after thermal exposure at 1300 °C in water vapor environment

within the load interval of 250-500 mN for both mullite and BSAS. At this point, it is hypothesized that the measured E values represent a macroscopic characteristic on the material (useful for engineering purposes) and not one of small volumes of its microstructure. Furthermore, the size of the indentation impressions at loads of 500 mN

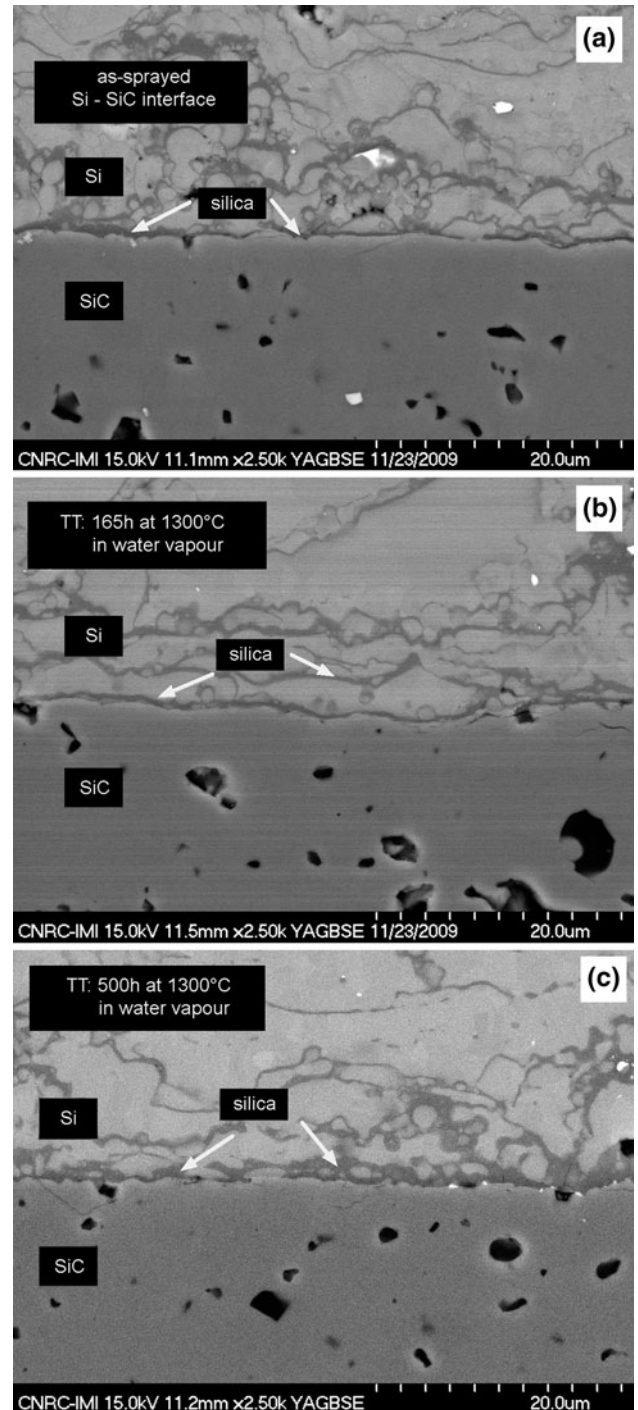


Fig. 4 SEM details of the interface between the Si bond coat and SiC substrate before and after thermal exposure at 1300 °C in water vapor environment

(i.e., triangle size $\sim 15 \mu\text{m}$, see Fig. 2) supports this hypothesis. Indeed, typical APS ceramic splats exhibit thicknesses in the order of $1 \mu\text{m}$ (Ref 17). Therefore, when areas representing triangular impression sizes of $\sim 15 \mu\text{m}$ are probed (i.e., volumes probed $\sim 80 \mu\text{m}^3$) a group of many splats is tested and not just one single or few, thus

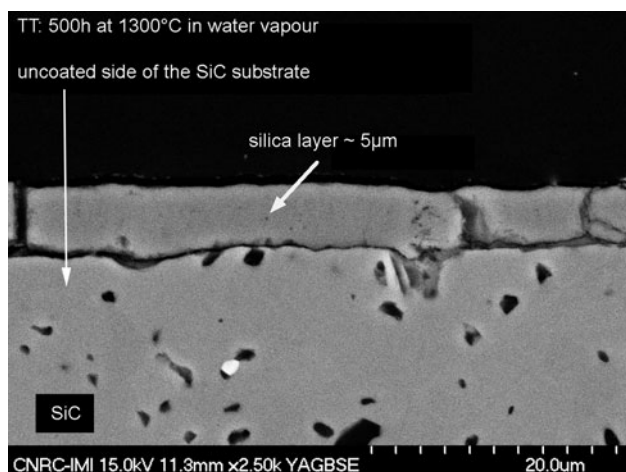


Fig. 5 SEM detail of the SiO_2 layer thermally grown on the uncoated SiC substrate

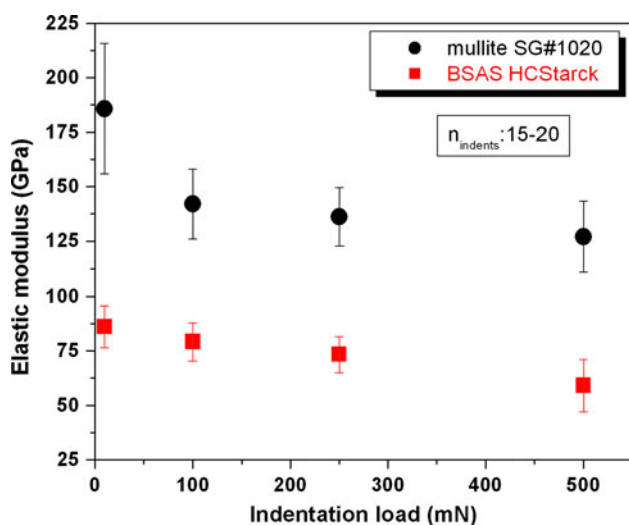


Fig. 6 E values versus indentation load (from 10 to 500 mN) for as-sprayed mullite and BSAS coatings

offering a more than local perspective of the coating's elastic modulus.

As an attempt to validate this hypothesis, the E value of a fully crystalline BSAS coating, sprayed directly on SiC substrate, was measured via laser-ultrasonics and compared with IIT measurements obtained using the 500 mN load. The choice for this ultrasonic technique is based on the fact that the E values measured by this approach do represent the overall coating microstructure. The comparative results are given in Table 2, where the E values obtained via laser-ultrasonics represent an average of 100 measurements. There is a fairly good agreement between the E values measured via IIT and laser-ultrasonics for the as-sprayed BSAS coatings confirming that the E values measured via IIT at 500 mN give a fair assessment of the macroscopic E values of the coatings.

Table 2 E values measured via IIT at 500 mN (50 gf) load and laser-ultrasonics for an as-sprayed BSAS coating

Coating	IIT 500 mN (50 gf) ($n = 15-20$)	Laser-ultrasonics (100 pulses)
BSAS	60 ± 12 GPa	65 ± 5 GPa

Based on these results, the evolution of E values as measured via IIT (at 50 gf load) from as-sprayed to thermally exposed EBCs at 1300 °C in water vapor environment (165 and 500 h) is shown in Fig. 7.

It can be observed that there is a significant growth in the E values of the mullite coating, from ~125 GPa (as-sprayed) to ~180 GPa after 500 h of isothermal exposure. This is an expected result for a ceramic material, where it was observed that the main increase in hardness, Young's modulus, and thermal diffusivity occurred during the initial hours of thermal exposure at, e.g., 1400 °C, followed by a more gradual increase with the time of annealing (Ref 18). On the other hand, the porosity levels of the coatings indicated little difference between the as-sprayed coatings and the thermally heated ones and thus the increase in both hardness and Young modulus was attributed to the improved inter-splat bonding and the disappearance of fine inter-splat pores produced by material diffusion. A similar trend is observed in this study for the mullite coatings.

The E value of the as-sprayed BSAS coating is about ~60 GPa. E values below 100 GPa can be considered as "low" for ceramic coatings. Indeed the E values for the BSAS coatings exhibited an unexpected high stability showing a rather steady evolution from ~60 to ~68 GPa after 500 h of thermal treatment as depicted in Fig. 7. In this case, the phenomena of closure effects (i.e., reduced inter-splat distance and increased contact) suggested in Ref 18 do not appear to play a significant role. This might be related to the much coarser pore size observed for BSAS in comparison to that of mullite (Fig. 3). In this study, the evolution of E values for the BSAS coatings was found to be as stable as the evolution of the BSAS coatings porosity (i.e., similar values for the as-sprayed and thermally exposed coatings). Nevertheless, further research will have to be done to explain in greater detail this dual stability for the BSAS.

Other authors have partially hypothesized the improved crack resistance and durability of BSAS EBCs are due to the "low" E values of these coatings (Ref 1, 2). This work reports such a low E value and confirms this hypothesis. The absence of significant phase transformation (Fig. 2) and the stability of the low elastic modulus values (Fig. 7) retained by the BSAS top layers even after harsh environmental exposures provides a plausible explanation for the almost crack-free coatings observed, as well as, their durability and effective SiC substrate protection. These characteristics were suggested and discussed by other authors (Ref 1, 2); although, the evolution of E values and XRD patterns for the EBCs were not reported at that point of time.

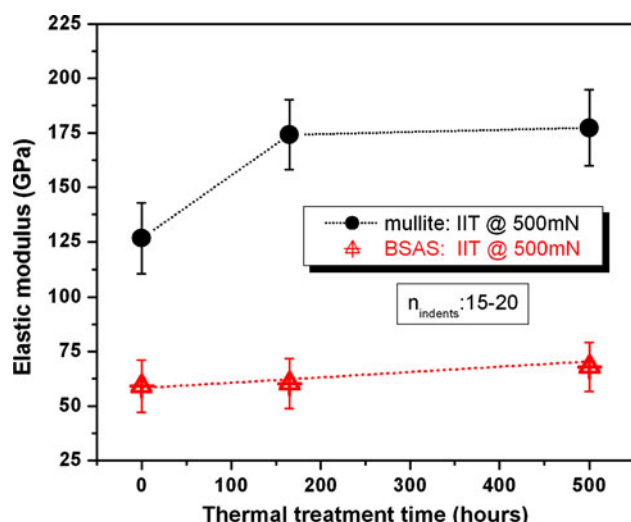


Fig. 7 Evolution of E values (IIT performed at 500 mN load) from as-sprayed to thermally exposed mullite and BSAS coatings at 1300 °C in water vapor environment, shown in Fig. 3(a)-(c)

4. Conclusions

In this work, the evolution of the coating microstructure and elastic moduli of fully crystalline Si, mullite, and BSAS (celsian phase) EBCs under high temperature exposure has been characterized. These tri-layer EBCs were found to be stable after thermal exposure at 1300 °C for up to 500 h in water vapor environment, i.e., no debonding, delamination, or significant through-thickness cracking was observed. The SiC substrate was effectively protected from oxidation and water vapor attack.

The fully crystalline as-sprayed BSAS coatings did not exhibit any significant phase transformation after thermal exposure to 1300 °C, in water vapor environment, up to 500 h. The as-sprayed and heat-treated coatings only exhibited the celsian phase of BSAS.

Elastic modulus for this EBC architecture has been assessed via instrumented indentation testing and laser ultrasonics. It should be pointed out that the E values of BSAS are almost stable from as-sprayed to thermally heated up to 500 h.

Previous works have attributed the improved crack resistance and durability of Si/mullite/BSAS EBCs to the low E values of the BSAS coatings and CTE match, which reduces thermo-mechanical stresses, as well as, the phase stability of fully crystalline BSAS coatings in water vapor environment. To the best knowledge of the authors, this is the first time that (i) the E values and (ii) the phase stability (via XRD) of as-sprayed and thermal-treated APS BSAS in water vapor environment are reported in the open literature. The results reported in this work tend to validate these previous statements.

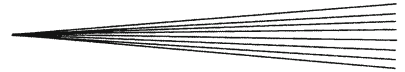
Acknowledgments

The authors would like to acknowledge valuable technical support from the Surface Technology Group

technical officers: J.-F. Alarie (metallographic preparation), S. Bélanger (plasma spraying), B. Harvey (EBC rig engineering), M. Lamontagne (thermal spray process monitoring) and M. Thibodeau (SEM characterization).

References

1. K.N. Lee, D.S. Fox, J.I. Eldridge, D. Zhu, R.C. Robinson, N.P. Bansal, and R.A. Miller, Upper Temperature Limit of Environmental Barrier Coatings Based on Mullite and BSAS, *J. Am. Ceram. Soc.*, 2003, **86**(8), p 1299-1306
2. N.S. Jacobson, D.S. Fox, J.L. Smialek, E.J. Opila, C. Dellacorte, and K.N. Lee, Performance of Ceramics in Severe Environments, *ASM Handbook—Corrosion: Materials*, Vol. 13B. S.D. Cramer and B.S. Covino Jr., Eds., ASM International, Materials Park, OH, USA, 2005, p 565-577
3. J. Kimmel, N. Miriyala, J. Price, K. More, P. Tortorelli, H. Eaton, G. Linsey, and E. Sun, Evaluation of CFCC Liners with EBC after Field Testing in a Gas Turbine, *J. Eur. Ceram. Soc.*, 2002, **22**, p 2769-2775
4. S. Latzel, R. Vaßen, and D. Stöver, New Environmental Barrier Coating System on Carbon-Fiber Reinforced Silicon Carbide Composites, *J. Therm. Spray Tech.*, 2005, **14**, p 268-272
5. K.N. Lee, D.S. Fox, and N.P. Bansal, Rare Earth Silicate Environmental Barrier Coatings for SiC/SiC Composites and Si₃N₄ Ceramics, *J. Eur. Ceram. Soc.*, 2005, **25**, p 1705-1715
6. E. Garcia, J. Mesquita-Guimarães, P. Miranzo, M.I. Osendi, Y. Wang, R.S. Lima, and C. Moreau, Mullite and Mullite/ZrO₂-7wt.%Y₂O₃ Powders for Thermal Spraying of Environmental Barrier Coatings, *J. Therm. Spray Technol.*, 2010, **19**(1-2), p 286-293
7. D. E. Glass, Ceramic Matrix Composite (CMC) Thermal Protection Systems (TPS) and Hot Structures for Hypersonic Vehicles., *15th American Institute of Aeronautics and Astronautics (AIAA) Space Planes and Hypersonic Systems and Technologies Conference*, PDF file #AIAA-2008-2682 at: http://ntrs.nasa.gov/archive/nasa/casi.ntrs.nasa.gov/20080017096_2008016802.pdf (October 12, 2009)
8. N.P. Bansal, Solid State Synthesis and Properties of Monoclinic Celsian, *J. Mater. Sci.*, 1998, **33**, p 4711-4715
9. J.I. Eldridge and K.N. Lee, Phase Evolution of BSAS in Environmental Barrier Coatings, *Ceram. Eng. Sci. Proc.*, 2001, **22**(4), p 383-390
10. T. Bhatia, H. Eaton, E. Sun et al., Advanced Environmental Barrier Coatings for SiC/SiC Composites, *Proc. ASME Turbo Expo*, 2005, **1**, p 253-258
11. B.J. Harder and K.T. Faber, Transformation Kinetics in Plasma-Sprayed Barium- and Strontium-Doped Aluminosilicate, *Scr. Mater.*, 2010, **62**(5), p 282-285
12. B.J. Harder, J.D. Almer, C.M. Weyant et al., Residual Stress Analysis of Multilayer Environmental Barrier Coatings, *J. Am. Ceram. Soc.*, 2009, **92**(2), p 452-459
13. W.C. Oliver and G.M. Pharr, Measurement of Hardness and Elastic Modulus by Instrumented Indentation: Advances in Understanding and Refinements to Methodology, *J. Mater. Res.*, 2004, **19**(1), p 3-20
14. C. Bescond, S.E. Kruger, D. Lévesque, R.S. Lima, and B.R. Marple, In-situ Simultaneous Measurement of Thickness Elastic Moduli and Density of Thermal Sprayed WC-Co Coatings by Laser-Ultrasonics, *J. Therm. Spray Technol.*, 2007, **16**(2), p 238-244
15. A.A. Elmustafaa and D.S. Stone, Nanoindentation and the Indentation Size Effect: Kinetics of Deformation and Strain Gradient Plasticity, *J. Mech. Phys. Solids*, 2003, **51**, p 357-381
16. B.-K. Jang, Influence of Low Indentation Load on Young's Modulus and Hardness of 4 mol% Y₂O₃-ZrO₂ by Nanoindentation, *J. Alloy Compd.*, 2006, **426**, p 312-315
17. S. Sampath, X.Y. Jiang, J. Matejicek, A.C. Leger, and A. Vardelle, Substrate Temperature Effects on Splat Formation, Microstructure Development and Properties of Plasma Sprayed



Coatings Part I: Case Study for Partially Stabilized Zirconia, *Mater. Sci. Eng. A*, 1999, **272**, p 181-188

18. B.R. Marple, R.S. Lima, C. Moreau, S.E. Kruger, L. Xie, and M.R. Dorfman, Yttria-Stabilized Zirconia Thermal

Barriers Sprayed Using N₂-H₂ and Ar-H₂ Plasmas: Influence of Processing and Heat Treatment on Coating Properties, *J. Therm. Spray Technol.*, 2007, **16**(5-6), p 791-797